An elastic interface model for mixed-mode fracture of adhesive joints

Stefano Bennati[1], Paolo S. Valvo[1]

[1]*Department of Civil Engineering (Structures), University of Pisa, Italy*
E-mail: s.bennati@ing.unipi.it, p.valvo@ing.unipi.it

Keywords: Adhesive joint, elastic interface, mixed-mode fracture.

SUMMARY. The paper presents a mechanical model of the single-lap joint (SLJ) test, where the adherends are considered as shear-deformable elastic laminated beams, partly connected by an elastic-brittle interface. The problem is described by a set of six coupled differential equations, which has been analytically solved, thus obtaining explicit expressions for the internal forces, interfacial stresses, energy release rate, and mode mixity angle.

1 INTRODUCTION

Adhesive joints are currently used to bond structural elements made of composite or traditional (metallic) materials [1]. Depending on the geometry and mechanical properties of adherends and adhesive, the ultimate load-carrying capacity of an adhesive joint is limited by several, interacting failure modes. These include, for instance, rupture of the adherends, failure in shear or peeling of the adhesive, and delamination of the adherends (when made of composite laminates).

Because of the relevance of the problem, many experimental test methods have been developed to evaluate the effectiveness of adhesive joints. The simplest test is probably the single-lap joint (SLJ) test [2, 3], used to assess the shear strength of adhesive joints. Actually, in the case of balanced joints (i.e. when the two adherends are identical in geometry and material), provided that the adherends are very rigid compared to the adhesive, failure occurs by the cracking of the adhesive layer under prevailing mode II fracture conditions. In general, however, mixed-mode fracture conditions apply [4]. Simple analytical models of the SLJ test were developed in the pioneering works of Volkersen [5] and Goland and Reissner [6]. A detailed literature survey on this topic has been recently given by da Silva *et al.* [7].

The present paper is intended as a further contribution to the study of adhesive joints in composite structures. Following a modelling approach similar to that developed elsewhere for the analysis of delamination [8], we have adopted a mechanical model of the single-lap joint test in which two structural elements, generally different the one from the other for thickness and material, are bonded by a single adhesive layer. The model considers the adherends as elastic laminated beams, partly connected by a deformable interface, here representing the adhesive layer. The shear deformability of the beams, which may be relevant for composite laminates, is considered according to Timoshenko's theory. The interface is considered as a continuous distribution of normal and tangential elastic-brittle springs, whose failure is governed by a mixed-mode crack-growth criterion.

A set of six coupled differential equations describes the problem. By adopting the interfacial stresses as principal unknowns, the original equation set is changed into two uncoupled higher-order differential equations. These equations are solved analytically and explicit expressions for the interfacial stresses and internal forces in the bonded elements are deduced. Finally, the energy release rate and mode-mixity angle at the ends of the adhesively bonded region are determined.

A numerical example is presented and a very first comparison with similar models available in the literature is carried out.

2   FORMULATION OF THE PROBLEM

2.1 *Mechanical model*

A scheme of the single-lap joint test is shown in Fig. 1. The specimen is composed of two adherends of width B (not shown in the figure) and thicknesses $H_1 = 2\,h_1$ and $H_2 = 2\,h_2$, generally made of different materials, bonded by an adhesive layer of thickness t over a portion of length b. During the test, the specimen is loaded in tension by two opposite forces of magnitude P.
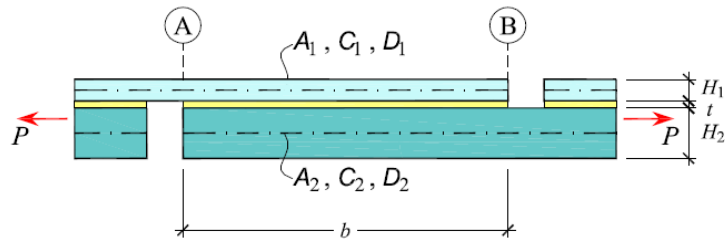
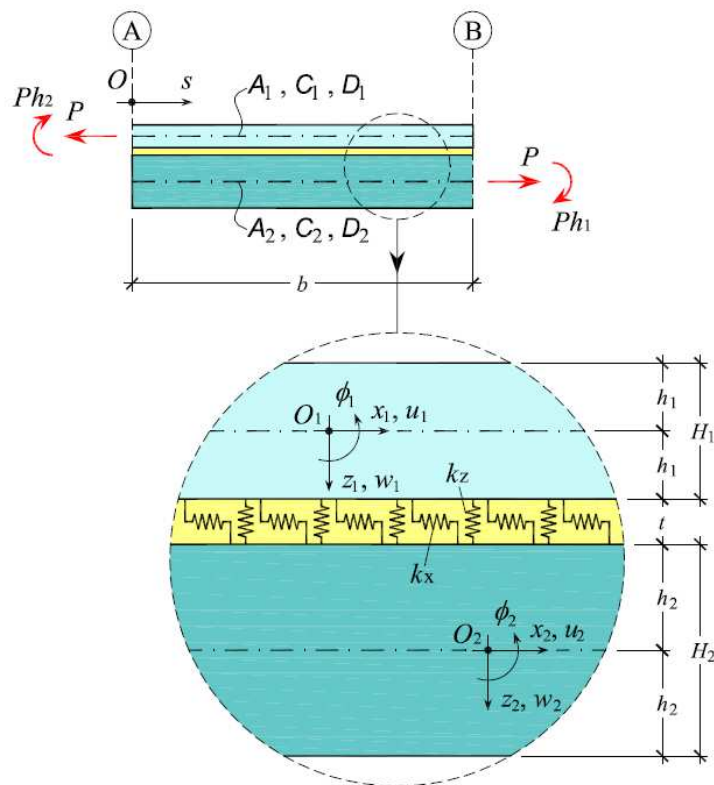Figure 1: Scheme of the single-lap joint test.

Figure 2: Mechanical model of the SLJ test.

In the mechanical model (Fig. 2a), the adherends behave as elastic laminated beams according to Timoshenko's theory. We denote with A_α, C_α and D_α their extensional, shear and bending stiffnesses, respectively (here, and in the following, $\alpha = 1$, 2 refer to the two adherends), computed as indicated by classical laminated plate theory [9]. The adhesive layer is represented by a deformable interface, consisting of a continuous distribution of elastic-brittle springs (Fig. 2b), with elastic constants k_z and k_x, respectively acting along the normal and tangential directions with respect to the interface plane. Rupture of the springs is governed by a mixed-mode crack-growth criterion in terms of the energy release rate. The generic cross section along the adhesively bonded region is specified by the abscissa s. Two local reference systems, $O_1x_1z_1$ and $O_2x_2z_2$, are defined with the origins on the centrelines of the adherends. Accordingly, we indicate with u_α and w_α the mid-plane displacements of the adherends along the axial and transverse directions, respectively, and with ϕ_α the rotations of their cross sections, positive if counter-clockwise (Fig. 2b).

2.2 Differential problem

The equilibrium equations for the adherends in the bonded portion ($s \in [0, b]$) are

$$\frac{dN_\alpha}{ds} + n_\alpha = 0, \quad \frac{dQ_\alpha}{ds} + q_\alpha = 0, \quad \frac{dM_\alpha}{ds} + m_\alpha - Q_\alpha = 0, \tag{1}$$

where N_α, Q_α, and M_α are respectively the axial force, shear force, and bending moment, and

$$n_1 = -n_2 = B\tau, \quad q_1 = -q_2 = B\sigma, \quad m_\alpha = B\tau h_\alpha \tag{2}$$

are the corresponding distributed loads and couples, and

$$\sigma = k_z \Delta w, \quad \tau = k_x \Delta u, \tag{3}$$

are the normal and tangential interfacial stresses. These are proportional to the axial and transverse relative displacements at the interface, $\Delta u = u_2^- - u_1^+$ and $\Delta w = w_2^- - w_1^+$, where u_1^+ and w_1^+ are the displacements at the bottom surface ($z_1 = h_1$) of adherend 1 and u_2^- and w_2^- are the displacements at the top surface ($z_2 = -h_2$) of adherend 2. The axial displacements of the adherends vary linearly with the thickness coordinate, so that $u_1^+ = u_1 + \phi_1 h_1$ and $u_2^- = u_2 - \phi_2 h_2$, while the transverse displacements are assumed constant throughout the thickness, so that $w_1^+ = w_1$ and $w_2^- = w_2$. Thus,

$$\Delta u = u_2 - u_1 - \phi_2 h_2 - \phi_1 h_1, \quad \Delta w = w_2 - w_1. \tag{4}$$

The constitutive laws for the adherends can be written as

$$N_\alpha = B A_\alpha \varepsilon_\alpha, \quad Q_\alpha = B C_\alpha \gamma_\alpha, \quad M_\alpha = B D_\alpha \kappa_\alpha, \tag{5}$$

where

$$\varepsilon_\alpha = \frac{du_\alpha}{ds}, \quad \gamma_\alpha = \phi_\alpha + \frac{dw_\alpha}{ds}, \quad \kappa_\alpha = \frac{d\phi_\alpha}{ds}, \tag{6}$$

are respectively the axial strain, shear strain, and curvature of the adherends.

By substituting Eqs. (2), (5), and (6) into (1), we get the set of governing differential equations,

$$
\frac{d^2 u_1}{ds^2} = -\frac{\tau}{A_1}, \quad \frac{d^2 w_1}{ds^2} + \frac{d\phi_1}{ds} = -\frac{\sigma}{C_1}, \quad \frac{d^3\phi_1}{ds^3} = -\frac{1}{D_1}(\sigma + h_1 \frac{d\tau}{ds}),
$$
$$
\frac{d^2 u_2}{ds^2} = \frac{\tau}{A_2}, \quad \frac{d^2 w_2}{ds^2} + \frac{d\phi_2}{ds} = \frac{\sigma}{C_2}, \quad \frac{d^3\phi_2}{ds^3} = \frac{1}{D_2}(\sigma - h_2 \frac{d\tau}{ds}),
$$

(7)

where the interfacial stresses, σ and τ, are given by Eqs. (3) and (4). The differential problem is completed by the boundary conditions

$$
N_1\big|_{s=0} = P, \quad Q_1\big|_{s=0} = 0, \quad M_1\big|_{s=0} = Ph_2; \quad N_1\big|_{s=b} = 0, \quad Q_1\big|_{s=b} = 0, \quad M_1\big|_{s=b} = 0;
$$
$$
N_2\big|_{s=0} = 0, \quad Q_2\big|_{s=0} = 0, \quad M_2\big|_{s=0} = 0; \quad N_2\big|_{s=b} = P, \quad Q_2\big|_{s=b} = 0, \quad M_2\big|_{s=b} = -Ph_1;
$$

(8)

which can be expressed in terms of the displacements, u_α, w_α and ϕ_α, by using Eqs. (5) and (6).

3 SOLUTION STRATEGY

3.1 *Change of variables*

Following a solution strategy similar to that of Ref. [8], we introduce a change of variables that simplifies strongly the analytical solution of the problem. Namely, we adopt the interfacial stresses as the main unknowns. To this aim, we substitute Eqs. (4) into (3) and then differentiate the resulting expressions for σ and τ with respect to s four and three times, respectively. Thus, we obtain a sixth-order linear homogeneous differential equation for the normal interfacial stress,

$$
\frac{d^6\sigma}{ds^6} + \hat{b}\frac{d^4\sigma}{ds^4} + \hat{c}\frac{d^2\sigma}{ds^2} + \hat{d}\,\sigma = 0 ,
$$

(9)

where the constant coefficients are

$$
\hat{b} = -k_x(a_1 + a_2 + d_1 h_1^2 + d_2 h_2^2) - k_z(c_1 + c_2),
$$
$$
\hat{c} = k_x k_z(a_1 + a_2 + d_1 h_1^2 + d_2 h_2^2)(c_1 + c_2) + k_z(d_1 + d_2),
$$
$$
\hat{d} = -k_x k_z[(a_1 + a_2)(d_1 + d_2) + d_1 d_2(h_1 + h_2)^2],
$$

(10)

and $a_\alpha = 1/A_\alpha$, $c_\alpha = 1/C_\alpha$, and $d_\alpha = 1/D_\alpha$ denote the extensional, shear and bending compliances of the adherends, respectively.

The tangential interfacial stress can then be obtained by integrating the following equation

$$
\frac{d\tau}{ds} = -\frac{1}{d_1 h_1 - d_2 h_2}[\frac{1}{k_z}\frac{d^4\sigma}{ds^4} - (c_1 + c_2)\frac{d^2\sigma}{ds^2} + (d_1 + d_2)\,\sigma].
$$

(11)

3.2 *Interfacial stresses*

The general solution to Eq. (9) can be written as

$$\sigma(s) = \sum_{i=1}^{6} F_i \exp(\lambda_i s), \tag{12}$$

where F_1, F_2, …, F_6 are integration constants to be determined by imposing the boundary conditions, and λ_1, λ_2, …, λ_6 are the roots of the characteristic equation,

$$\lambda^6 + \hat{b}\lambda^4 + \hat{c}\lambda^2 + \hat{d} = 0. \tag{13}$$

By substituting Eq. (12) into (11) and integrating, we obtain the general solution for the tangential stress,

$$\tau(s) = -\frac{1}{d_1 h_1 - d_2 h_2} \left\{ \sum_{i=1}^{6} F_i [\frac{\lambda_i^3}{k_z} - (c_1 + c_2)\lambda_i + (d_1 + d_2)\frac{1}{\lambda_i}]\exp(\lambda_i s) + F_7 \right\}, \tag{14}$$

where F_7 is another constant.

3.3 *Integration constants*

The internal forces can now be deduced by substituting the expressions for the interfacial stresses (12) and (14) into Eqs. (2) and (1), and integrating the latter with respect to *s*. This process yields the analytical expressions for the internal forces, where six new integration constants, F_8, F_9, …, F_{13}, appear. In turn, the expressions for the internal forces are substituted into the constitutive laws (5). Then, by using Eqs. (6) and integrating with respect to *s*, the analytical expressions for the displacements are also deduced. These involve six more constants, F_{14}, F_{15}, …, F_{19}.

To sum up, there are 19 integration constants to be determined, but the boundary conditions (8) appear insufficient because they consist of only 12 equations. Actually, by introducing the obtained expressions for the interfacial stresses and displacements into Eqs. (3), we find 7 relations between the constants, only 12 of which turn out to be independent of each other. So, by imposing boundary conditions (8), we find the values of all the integration constants, except for F_{14}, F_{16}, and F_{18}, which represent a rigid displacement of the whole system.

In particular, the first six constants are obtained by solving a linear equation set,

$$
\begin{aligned}
&\sum_{i=1}^{6} (\frac{\lambda_i^2}{k_z} - c_1 - c_2) f_i = d_1 h_2, \\
&\sum_{i=1}^{6} \frac{f_i}{\lambda_i} = 0, \\
&\sum_{i=1}^{6} \frac{f_i}{\lambda_i^2} = -\frac{(a_1 d_2 + a_2 d_1) h_2 - a_1 d_1 (h_1 - h_2) + d_1 d_2 h_2^2 (h_1 + h_2)}{(a_1 + a_2)(d_1 + d_2) + d_1 d_2 (h_1 + h_2)^2}, \\
&\sum_{i=1}^{6} (\frac{\lambda_i^2}{k_z} - c_1 + c_2) \exp(\lambda_i b) f_i = d_2 h_1, \\
&\sum_{i=1}^{6} \frac{\exp(\lambda_i b)}{\lambda_i} f_i = 0, \\
&\sum_{i=1}^{6} \frac{\exp(\lambda_i b)}{\lambda_i^2} f_i = -\frac{(a_1 d_2 + a_2 d_1) h_1 + a_2 d_2 (h_1 - h_2) + d_1 d_2 h_1^2 (h_1 + h_2)}{(a_1 + a_2)(d_1 + d_2) + d_1 d_2 (h_1 + h_2)^2},
\end{aligned}
\tag{15}
$$

where $f_i = F_i B / P$, $i = 1, 2, \ldots, 6$.

3.4 *Internal forces*

Based on the above results, we deduce the expressions for the internal forces in the adherends:

$$
N_1(s) = P \frac{a_2(d_1 + d_2) + d_1 d_2 h_1 (h_1 + h_2)}{(a_1 + a_2)(d_1 + d_2) + d_1 d_2 (h_1 + h_2)^2} + P \frac{\sum_{i=1}^{6} f_i (\frac{\lambda_i^2}{k_z} - c_1 - c_2 + \frac{d_1 + d_2}{\lambda_i^2}) \exp(\lambda_i s)}{d_1 h_1 - d_2 h_2}, \tag{16}
$$
$$
N_2(s) = P - N_1(s),
$$

for the axial forces;

$$
Q_1(s) = -P \sum_{i=1}^{6} \frac{f_i}{\lambda_i} \exp(\lambda_i s), \quad Q_2(s) = -Q_1(s), \tag{17}
$$

for the shear forces; and lastly,

$$
M_1(s) = -P \frac{(a_1 h_1 - a_2 h_2) d_2}{(a_1 + a_2)(d_1 + d_2) + d_1 d_2 (h_1 + h_2)^2} + P \frac{\sum_{i=1}^{6} f_i [(\frac{\lambda_i^2}{k_z} - c_1 - c_2) h_1 + \frac{d_2 (h_1 + h_2)}{\lambda_i^2}] \exp(\lambda_i s)}{d_1 h_1 - d_2 h_2}, \tag{18}
$$
$$
M_2(s) = -M_1(s) + N_1(s) h_2 - N_2(s) h_1,
$$

for the bending moments. Likewise, explicit expressions for the displacements can be obtained. For simplicity, we omit here those results, which will be presented in an extended paper.

3.5 *Energy release rate, crack-tip interfacial stresses, and mode mixity*

Failure of a real adhesive joint can occur as a consequence of several different failure modes. Here, we focus on the failure due to the cracking of the adhesive layer. In this case, crack growth can initiate at either of the two sections, *A* and *B*, at the ends of the bonded region, where the interfacial stresses attain peak values,

$$
\sigma_A = \sigma\big|_{s=0} = \frac{P}{B}\sum_{i=1}^{6} f_i, \qquad\qquad \sigma_B = \sigma\big|_{s=b} = \frac{P}{B}\sum_{i=1}^{6} f_i \exp(\lambda_i b),
$$

$$
\tau_A = \tau\big|_{s=0} = \frac{P}{B}\frac{\sum_{i=1}^{6} f_i \lambda_i (c_1 + c_2 - \frac{\lambda_i^2}{k_z})}{d_1 h_1 - d_2 h_2}, \quad \tau_B = \tau\big|_{s=b} = \frac{P}{B}\frac{\sum_{i=1}^{6} f_i \lambda_i (c_1 + c_2 - \frac{\lambda_i^2}{k_z})\exp(\lambda_i b)}{d_1 h_1 - d_2 h_2}. \tag{19}
$$

Accordingly, the energy release rates at the two potential crack tips are

$$
G_A = G_{A,\mathrm{I}} + G_{A,\mathrm{II}} \qquad \text{and} \qquad G_B = G_{B,\mathrm{I}} + G_{B,\mathrm{II}}, \tag{20}
$$

where

$$
G_{A,\mathrm{I}} = \frac{\sigma_A^2}{2k_z}, \quad G_{A,\mathrm{II}} = \frac{\tau_A^2}{2k_x} \qquad \text{and} \qquad G_{B,\mathrm{I}} = \frac{\sigma_B^2}{2k_z}, \quad G_{B,\mathrm{II}} = \frac{\tau_B^2}{2k_x}, \tag{21}
$$

are the respective contributions of modes I and II to the energy release rate. Finally, we obtain the mode-mixity angles at the two endpoints,

$$
\psi_A = \arctan\sqrt{\frac{G_{A,\mathrm{II}}}{G_{A,\mathrm{I}}}} \qquad \text{and} \qquad \psi_B = \arctan\sqrt{\frac{G_{B,\mathrm{II}}}{G_{B,\mathrm{I}}}}, \tag{22}
$$

from which the critical values of the energy release rate,

$$
G_{A,\mathrm{c}} = G_{\mathrm{c}}(\psi_A) \qquad \text{and} \qquad G_{B,\mathrm{c}} = G_{\mathrm{c}}(\psi_B), \tag{23}
$$

can be computed according to some chosen mixed-mode crack-growth criterion [4], suitable for the adhesive under examination.

4 NUMERICAL EXAMPLE

By way of illustration, we apply the proposed model to the case of a balanced (symmetric) SLJ already considered for comparison purposes by das Neves *et al.* [10]. The adherends have width $B = 25$ mm and thickness $H_1 = H_2 = 2$ mm. The adhesive layer has length $b = 50$ mm and thickness $t = 1$ mm. The elastic moduli of the adherends (here assumed isotropic) are $E_1 = E_2 = 106.3$ GPa, $G_1 = G_2 = 40.0$ GPa, the moduli of the adhesive are $E_a = 4.44$ GPa and $G_a = 1.64$ GPa. Hence, the stiffnesses of the adherends turn out to be the following: $A_1 = E_1 H_1 = 212600$ N/mm ($= A_2$), $C_1 = 5\, G_1 H_1 / 6 = 66604$ N/mm ($= C_2$), $D_1 = E_1 H_1^3 / 12 = 70867$ N mm ($= D_2$).

As far as the elastic constants of the interface are concerned, similar models available in the literature consider these constants to be functions of the elastic moduli of the adhesive. Here, in order to account also for the localised deformation occurring at the crack-tip, which may be

particularly relevant for composite, orthotropic materials, we set

$$k_x = \frac{1}{\dfrac{h_1}{G_1} + \dfrac{t}{G_a} + \dfrac{h_2}{G_2}} = 1519.4 \,\frac{\text{N}}{\text{mm}^3} \quad \text{and} \quad k_z = \frac{1}{\dfrac{h_1}{E_1} + \dfrac{t}{E_a} + \dfrac{h_2}{E_2}} = 4097.7 \,\frac{\text{N}}{\text{mm}^3}. \quad (24)$$

Fig. 3 shows the internal forces in the upper (continuous, red curves) and lower (dashed, blue curves) adherends as functions of the abscissa, s, as given by Eqs. (16)–(18) for an applied load $P = 5$ kN. In particular, Fig. 3a shows the axial forces, N_1 and N_2, Fig. 3b represents the shear forces, Q_1 and Q_2, and Fig. 3c shows the bending moments, M_1 and M_2. In this case, the symmetry of the specimen is reflected into the symmetry of the plots of the internal forces.
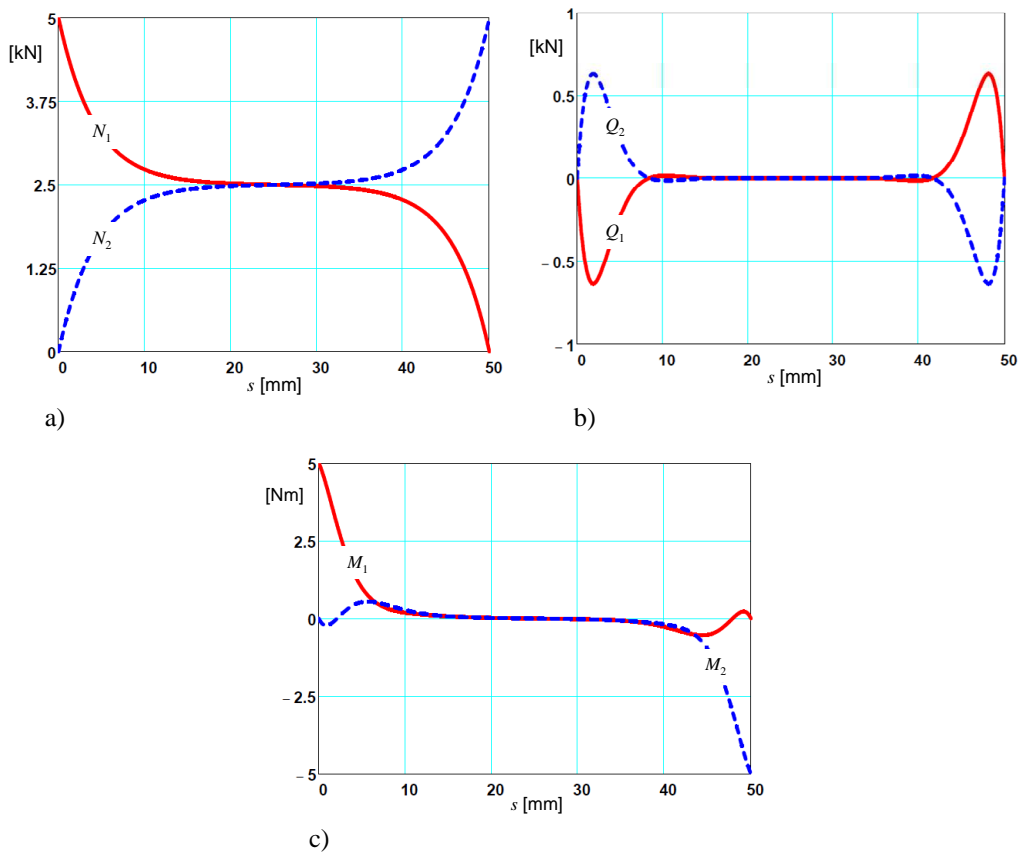

a)

b)

c)

Figure 3: Internal forces in the adherends.

Fig. 4 shows the normal and tangential interfacial stresses, σ and τ, as given by Eqs. (12) and (14), respectively, as functions of the abscissa, s. Both stress components attain peak values at the ends of the adhesively bonded region. The peak stress values obtained by the present model are compared in Table 1 with the corresponding values predicted by the models of Refs. [10] and [11]. A very good agreement is found for the peak tangential stress, while higher discrepancies emerge for the normal stress.
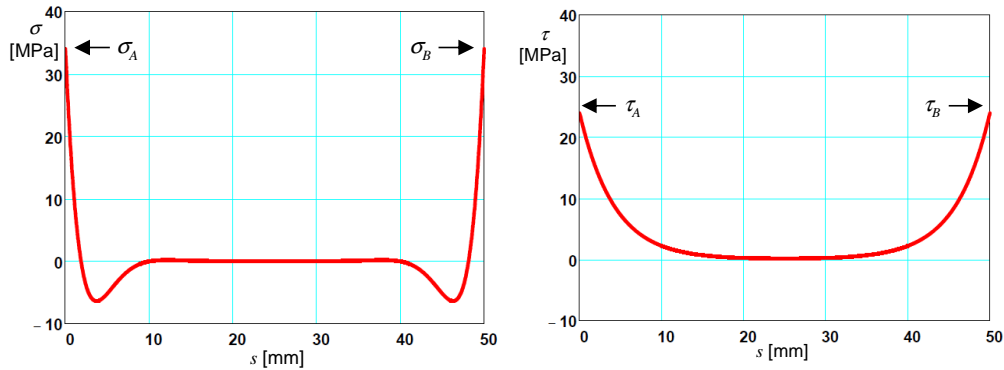
Figure 4: Normal and tangential interfacial stresses.

Table 1: Peak values of the interfacial stresses [MPa].

Stress component	Present model, Eqs. (19)	das Neves et al. [10]	Frostig et al. [11]
$\sigma_A = \sigma_B$	34.0	15.0	40.0
$\tau_A = \tau_B$	23.9	24.0	23.0

Correspondingly, we compute the mode I and II contributions to the energy release rate,

$$G_{A,I} = G_{B,I} = 141.1 \frac{J}{m^2} \quad \text{and} \quad G_{A,II} = G_{B,II} = 188.2 \frac{J}{m^2}, \qquad (25)$$

and the mode-mixity angle,

$$\psi_A = \psi_B = 49.1°, \qquad (26)$$

which show, at least in this case, that the contribution from mode I fracture is not negligible at all.

Lastly, as a first step towards the analysis of unbalanced SLJ specimens, in Fig. 5 we show the effect on the axial force N_1 of varying the ratio $\eta = H_1/H_2$, while keeping constant the overall thickness, $H_1 + H_2$.
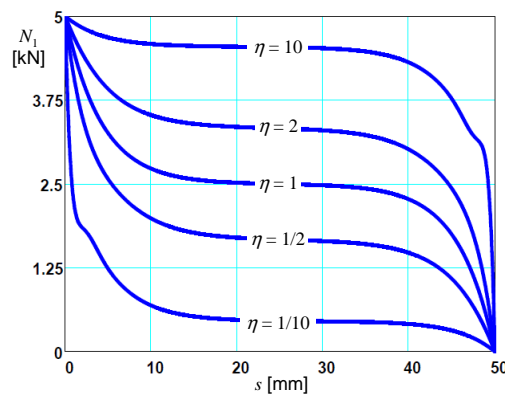

Figure 5: Axial force in the upper adherend for unbalanced (asymmetric) SLJ specimens.

5 CONCLUSIONS

We have presented a mechanical model of the single-lap joint (SLJ) test, suitable for balanced and unbalanced joints. The model considers the adherends as shear-deformable elastic laminated beams, partly connected by an elastic-brittle interface.

A complete explicit solution of the problem has been obtained for the internal forces and interfacial stresses. Hence, explicit expression for the energy release rate and mode mixity angle have also been deduced. The solution enables investigating the role of the relevant mechanical parameters, such as the dimensions of the specimen, the thicknesses and mechanical properties of the adherends and adhesive.

From the first carried out comparisons, a good agreement has been found between the theoretical predictions of our model and similar ones proposed in the literature. However, further work is necessary to allow the model to take into account some important aspects of the behaviour of real adhesive joints such as, for instance, the viscous and elastic-plastic behaviour of the adhesive, the geometrical non-linearity, due to large displacements, and the interaction of several failure modes. It is likely that the above improvements will require the use of numerical solution methods, for which the developed analytical solution will hopefully serve as a reliable basis.

References
[1] Adams, R.D. and Wake, W.C., *Structural adhesive joints in engineering*, Elsevier, London-New York (1984).
[2] ASTM D 1002-05, *Standard Test Method for Apparent Shear Strength of Single-Lap-Joint Adhesively Bonded Metal Specimens by Tension Loading (Metal-to-Metal)*.
[3] ASTM D3165-07, *Standard Test Method for Strength Properties of Adhesives in Shear by Tension Loading of Single-Lap-Joint Laminated Assemblies*.
[4] Hutchinson, J.W. and Suo, Z., "Mixed mode cracking in layered materials", *Advances in Applied Mechanics*, **29**, 63–191 (1992).
[5] Volkersen, O., "Die Nietkraftverteilung in zugbeanspruchten Nietverbindungen mit konstanten Laschenquerschnitten", *Luftfahrtforschung*, **15**, 45–47 (1938).
[6] Goland, M. and Reissner, E., "The Stresses in Cemented Joints", *ASME J. of Applied Mechanics*, **11**, A17-A27 (1944).
[7] da Silva, L.F.M., das Neves, P.J.C., Adams, R.D. and Spelt, J.K., "Analytical models of adhesively bonded joints – Part I: Literature survey", *Int. J. of Adhesion and Adhesives*, **29**, 319–330 (2009).
[8] Bennati, S., Colleluori, M., Corigliano, D. and Valvo, P.S., "An enhanced beam-theory model of the asymmetric double cantilever beam (ADCB) test for composite laminates", *Composites Science and Techology*, **69**, 1735–1745 (2009).
[9] Jones, R.M., *Mechanics of composite materials –2nd ed.*, Taylor & Francis Inc., Philadelphia, PA (1999).
[10] das Neves, P.J.C., da Silva, L.F.M. and Adams, R.D., "Analysis of Mixed Adhesive Bonded Joints – Part I: Theoretical Formulation", *J. of Adhesion Science and Technology*, **23**, 1–34 (2009).
[11] Frostig, Y., Thomsen, O.T. and Mortensen, F., "Analysis of Adhesive-Bonded Joints, Square-End, and Spew-Fillet – High-Order Theory Approach", *J. Engineering Mechanics*, **125**, 1298–1307 (1999).